genes

MDPI

Article

Multi-Cohort Transcriptomic Analysis of Cell-Cycle Programs Associated with Pathological Grade in Intraductal Papillary Mucinous Neoplasms

Han Ren, Qianwei Cheng and Zhili Ji *

Beijing Chao-Yang Hospital, Capital Medical University, Beijing 100020, China
* Correspondence: anzhenjzl@mail.ccmu.edu.cn

Abstract

Background: Intraductal papillary mucinous neoplasms (IPMNs) are important pancreatic precursor lesions with heterogeneous risks of malignant progression. Although previous studies have revealed molecular heterogeneity among IPMNs, grade-associated transcriptional programs with consistent behavior across cohorts remain incompletely characterized. **Methods**: Public transcriptomic datasets from the Gene Expression Omnibus database were analyzed using a multi-cohort framework. Differential expression analysis and gene set enrichment analysis (GSEA) were performed in the discovery cohort (GSE63104) to identify transcriptional programs associated with high-risk IPMN lesions. Enrichment direction and specimen-level grade associations were assessed in an independent cohort of 28 microdissected foci from 14 patients (GSE26647). Sample-level pathway activity was quantified using single-sample GSEA (ssGSEA) in 24 IPMN specimens from GSE210351, and a composite proliferative program score was generated to assess associations with pathological grade and histological subtype. **Results**: GSEA identified three cell-cycle-associated Hallmark pathways, including HALLMARK_E2F_TARGETS, HALLMARK_G2M_CHECKPOINT, and HALLMARK_MITOTIC_SPINDLE, which were integrated as a proliferative transcriptional program. All three pathways showed concordant positive enrichment in GSE26647, where an independently implemented focus-level score also retained a positive grade association after exclusion of invasive foci. In the GSE210351 cohort, the composite proliferative program score was significantly increased in high-grade IPMNs compared with low-grade lesions. Multivariable linear regression further indicated that pathological grade and histological subtype were independently associated with proliferative program activity. In the 24 IPMN cases, the original GSVA-derived composite reproduced the overall grade difference, with an exact Wilcoxon p value of 0.0029. A noninvasive-only patient-clustered sensitivity analysis of GSE26647 retained the positive grade association. The grade-by-subtype interaction was not significant, and an epithelial-marker-adjusted model retained a positive grade coefficient. **Conclusions**: A grade-associated proliferative transcriptional pattern characterized by coordinated enrichment of E2F targets, G2M checkpoint, and mitotic spindle pathways is associated with IPMN pathological grade. These results characterize a tissue-level transcriptional correlate of pathological grade; its clinical discrimination and single-patient transferability require independent assessment.

Keywords: intraductal papillary mucinous neoplasm; pancreatic precursor lesion; transcriptomic analysis; cell cycle; multi-cohort replication

Check for updates

Academic Editors: Quan Zou and Albert Jeltsch

Received: 25 September 2026
Revised: 16 November 2026
Accepted: 24 November 2026
Published: 27 November 2026

Copyright: © 2026 by the authors. Licensee MDPI, Basel, Switzerland. This article is an open access article distributed under the terms and conditions of the Creative Commons Attribution (CC BY) license.

1. Introduction

Pancreatic cystic lesions are increasingly detected in clinical practice, partly due to the widespread use of cross-sectional imaging and the aging population. A recent systematic review and meta-analysis demonstrated that pancreatic cystic lesions are frequently identified on magnetic resonance imaging, with prevalence increasing substantially with age [1]. Among these lesions, intraductal papillary mucinous neoplasms (IPMNs) represent clinically important precursor lesions of pancreatic ductal adenocarcinoma (PDAC) [2]. IPMNs encompass a spectrum of pathological changes ranging from low-grade dysplasia to high-grade dysplasia and, in a subset of cases, invasive carcinoma [2,3]. Their heterogeneous potential for malignant progression makes accurate risk stratification of individual IPMNs an important clinical challenge.

Current clinical management of IPMNs relies largely on morphological features, clinical characteristics, and the presence of high-risk stigmata or worrisome features to estimate the likelihood of high-grade dysplasia or invasive carcinoma [3]. These criteria provide an important framework for surveillance and surgical decision-making; however, the biological behavior of IPMNs is heterogeneous, and molecular studies have revealed distinct biological features among lesions with different pathological states [4]. Increasing molecular studies have revealed substantial heterogeneity among IPMNs at genomic, transcriptomic, and cellular levels. Integrated molecular characterization has demonstrated distinct molecular features across IPMNs, while single-cell transcriptomic analyses have further revealed heterogeneous epithelial and microenvironmental states during neoplastic progression from precursor lesions toward invasive cancer [4,5]. In addition, genomic analyses have demonstrated the presence of multiple independent neoplastic clones with distinct mutational profiles, further highlighting the genetic complexity of IPMNs [6]. These observations suggest that pathological progression of IPMNs may involve coordinated alterations across multiple biological processes rather than changes in isolated genes alone.

Previous transcriptomic studies have identified gene expression changes associated with IPMN progression, including alterations in biological processes related to cell proliferation, hypoxia, epithelial-to-mesenchymal transition, and transforming growth factor-β signaling [7]. More recent integrated molecular analyses have further suggested that high-grade IPMNs exhibit activation of oncogenic transcriptional programs, including MYC-related signaling and cell-cycle-associated pathways [4]. These findings support the value of transcriptome-based approaches for characterizing molecular changes accompanying pathological progression. However, individual gene-level alterations alone may not fully capture coordinated biological activity across functionally related genes. Furthermore, the reproducibility of such transcriptional programs across independent IPMN cohorts remains insufficiently explored. Pathway-level analysis can therefore provide a complementary framework for identifying reproducible transcriptional programs associated with IPMN progression.

In this study, we sought to identify transcriptional programs associated with pathological progression of IPMNs and to assess their reproducibility across independent public datasets. We first performed differential expression analysis and gene set enrichment analysis in GSE63104 to identify biological pathways associated with high-risk IPMN lesions. The reproducibility of the identified pathways was then evaluated in the independent GSE26647 cohort. Finally, sample-level pathway activity was quantified in GSE210351 using single-sample gene set enrichment analysis, and the activity of the proliferative transcriptional program was summarized using a composite score to evaluate its association with pathological grade and histological subtype. Through this multi-cohort analytical framework, we aimed to determine whether a coordinated proliferative transcriptional program could be reproducibly associated with pathological progression across independent IPMN datasets.

2. Materials and Methods

2.1. Public Transcriptomic Datasets and Study Design

Publicly available transcriptomic datasets of pancreatic lesions were obtained from the Gene Expression Omnibus (GEO) database. Three independent datasets were included in the present study. Detailed characteristics of the three transcriptomic datasets are summarized in Table 1 and Supplementary Table S1. GSE63104 was used as the discovery cohort to identify transcriptional programs associated with high-risk and low-risk IPMN tissues. GSE26647 was used as an independent replication cohort to evaluate the reproducibility of the identified proliferation-associated pathways. GSE210351 was subsequently used for sample-level pathway activity scoring and evaluation of associations between proliferative program activity and pathological grade and histological subtype among IPMN samples.

Table 1. Characteristics, group definitions, and analytical roles of the GEO datasets.

GEO Cohort	Platform	Analytical Specimens and Group Definitions	Role
GSE63104	GPL15048; Affymetrix Rosetta/Merck HuRSTA array	23 IPMN specimens: low-risk $n = 6$, high-risk $n = 17$. High-risk includes high-grade dysplasia and invasive carcinoma.	Discovery
GSE26647	GPL5175; Affymetrix Human Exon 1.0 ST array	28 microdissected foci from 14 patients: low-grade $n = 10$, moderate-grade $n = 5$, high-grade $n = 6$, invasive carcinoma $n = 7$. LMD $n = 15$; HgInv $n = 13$.	Enrichment replication
GSE210351	GPL24676; Illumina NovaSeq 6000 RNA sequencing	24 IPMN specimens within a 41-specimen series: gastric low-grade $n = 6$, gastric high-grade $n = 6$, intestinal low-grade $n = 6$, intestinal high-grade $n = 6$.	Grade and subtype scoring

The analytical cohorts comprised 23 IPMN specimens in GSE63104, 28 microdissected histological foci from 14 patients in GSE26647, and 24 gastric-type or intestinal-type IPMN specimens selected from 41 profiled specimens in GSE210351. The sampling unit and pathological definitions were retained as recorded in the originating GEO studies.

The overall analytical workflow is illustrated in Figure 1 and consisted of four major steps: (1) differential expression analysis and gene set enrichment analysis (GSEA) in the discovery cohort; (2) independent enrichment replication and patient-clustered specimen-level comparisons in GSE26647; (3) sample-level quantification of pathway activity and construction of a composite proliferative program score in GSE210351; and (4) evaluation of the association between the composite score and pathological characteristics using univariable comparisons and multivariable linear regression.

2.2. Differential Expression Analysis and GSEA in the Discovery Cohort

GSE63104 was used as the discovery cohort. IPMN samples were classified into high-risk and low-risk groups according to the original risk classification defined in the source study. Differential expression analysis between high-risk and low-risk IPMN samples was performed using the limma package in R. Genes were ranked according to the moderated t-statistic, with positive values indicating higher expression in the high-risk group. According to the GEO deposition, the processed discovery array signals were robust multichip average normalized and log2 transformed. The original study defined the high-risk category by high-grade dysplasia or invasive carcinoma and the low-risk category by low-grade or moderate-grade dysplasia.

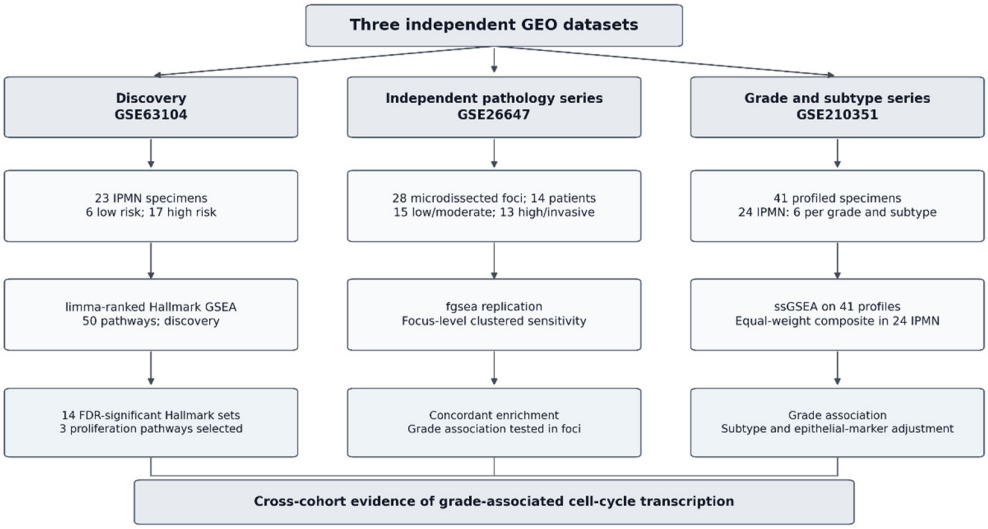

Figure 1. Study design and analytical workflow. Three independent GEO cohorts were analyzed using distinct but complementary strategies. GSE63104 included 23 IPMN specimens and was used for discovery of grade-associated Hallmark enrichment. GSE26647 included 28 laser-capture microdissected foci from 14 patients and was used for independent enrichment comparison and patient-clustered sensitivity analyses. GSE210351 included 41 profiled specimens, of which 24 grade-annotated gastric-type and intestinal-type IPMN specimens were assessed using the archived composite score. The analyses assessed pathology-associated transcriptional patterns rather than validated clinical prediction.

Gene set enrichment analysis was performed using the fgsea package with the ranked gene list generated from limma analysis and Hallmark gene sets obtained from the Molecular Signatures Database (MSigDB, version 7.5.1). Gene sets containing fewer than 15 or more than 500 genes were excluded. Enrichment was evaluated using normalized enrichment scores (NES), and multiple-testing correction was performed using the false discovery rate (FDR). Results for the full set of 50 Hallmark pathways in both discovery and replication cohorts, including enrichment scores, normalized enrichment scores, raw p values, and false discovery rates, are reported in Supplementary Tables S1 and S2. The original fgsea output was retrieved from the saved R analysis workspace. MSigDB Hallmark version 7.5.1 was retained to reproduce the original enrichment analysis, maintain identical pathway membership across the two archived cohorts, and preserve comparability with the saved leading-edge results. Its use supports internal reproducibility rather than equivalence with current gene set releases.

Three cell-cycle and mitosis-related Hallmark pathways, namely HALLMARK_E2F_TARGETS, HALLMARK_G2M_CHECKPOINT, and HALLMARK_MITOTIC_SPINDLE, were selected as the core proliferative transcriptional program based on their significant enrichment and biological relevance for subsequent validation and phenotype association analyses. The three Hallmark sets describe related stages of proliferation and contain shared genes. Their combination was used to summarize coordinated cell-cycle activity as one descriptive axis rather than three statistically independent biological processes. The original Hallmark membership lists contained 73 genes shared by E2F targets and G2M checkpoint, 19 by E2F targets and mitotic spindle, and 39 by G2M checkpoint and mitotic spindle. The equal-weight composite was compared with each individual score and three alternative weightings as a sensitivity analysis, rather than being assumed to improve discrimination.

2.3. Independent Replication of Enrichment in GSE26647

GSE26647 was used for independent assessment of enrichment direction and specimen-level grade contrasts. Based on the original dataset annotation, samples were classified into

low- and moderate-grade dysplasia (LMD) and high-grade dysplasia or invasive carcinoma (HgInv), following the pathological categories of the source study annotation. The LMD category included 10 low-grade and 5 moderate-grade foci, whereas HgInv included 6 high-grade and 7 invasive foci. The 28 microdissected foci were derived from 14 patients, and several patients contributed more than one histological grade.

Genes were ranked according to differential expression statistics between the two groups, with positive values representing higher expression in high-risk lesions. Gene set enrichment analysis was performed using the same fgsea framework, Hallmark gene sets, and filtering criteria as in the discovery cohort. The enrichment of HALLMARK_E2F_TARGETS, HALLMARK_G2M_CHECKPOINT, and HALLMARK_MITOTIC_SPINDLE was evaluated using normalized enrichment scores (NES) and false discovery rate (FDR). Concordant positive enrichment patterns of these three pathways across the discovery and validation cohorts were interpreted as evidence supporting the reproducibility of the proliferative transcriptional program. Replication was assessed at the level of enrichment direction and magnitude; no out-of-sample discrimination or prognostic classification performance was estimated from this comparison. For the secondary specimen-level analysis, the GSE26647 processed matrix was mapped using the GPL5175 transcript-cluster annotation. A single-gene annotation was required; where several transcript clusters mapped to one gene, the cluster with the greatest interquartile expression range was selected. A rank-based enrichment score was calculated for each of the three Hallmark gene sets, transformed to a within-cohort z score, and averaged. Ordinary least-squares grade contrasts were estimated with patient-clustered standard errors and t inference based on 13 degrees of freedom. The noninvasive subset excluded seven invasive foci, retaining six high-grade and 15 lower-grade foci from 14 patients. This sensitivity analysis used an explicitly specified rank-based implementation and was kept separate from the original GSVA-derived GSE210351 scoring procedure. The implementation in GSE26647 provides an independent within-cohort association test and is not an external validation of the numerical GSE210351 score scale.

2.4. Sample-Level Pathway Activity and Construction of the Composite Score

GSE210351 was used for sample-level quantification of the proliferative transcriptional program and subsequent pathological association analyses. Single-sample gene set enrichment analysis (ssGSEA) was performed using the GSVA package in R based on the three Hallmark pathways identified in the discovery cohort: HALLMARK_E2F_TARGETS, HALLMARK_G2M_CHECKPOINT, and HALLMARK_MITOTIC_SPINDLE. Among the 41 profiled specimens deposited under GSE210351, 24 gastric-type and intestinal-type IPMN specimens were selected for the pathological association analyses, with six low-grade and six high-grade lesions in each subtype. The original R command history confirms that ssGSEA was computed using the GSVA ssgseaParam interface and the variance-stabilized, batch-corrected expression matrix. The three pathway-specific ssGSEA calculations were applied to all 41 GSE210351 samples before the IPMN subgroup was selected.

For pathological association analyses, only IPMN samples with available pathological grade and histological subtype information were included. For each pathway, the resulting ssGSEA scores were z-score transformed across all 41 profiled specimens prior to restriction to the 24 IPMN cases. A composite proliferative program score was then calculated as the mean of the three standardized pathway scores: Each standardized pathway score was assigned a coefficient of one-third. This equal-weight summary was not fitted to pathological outcomes, and it is presented as a descriptive index rather than an optimized risk-prediction model. The archived R workspace contains the original three ssGSEA scores and their standardized values for all 41 samples. All reported GSE210351 inferential analyses used the

resulting archived composite scores for the 24 grade-annotated IPMN specimens. Because standardization used the full 41-specimen reference distribution, a stand-alone score for an additional patient would require fixed reference means and standard deviations and prospectively specified preprocessing. The present composite is therefore an exploratory cohort-relative index.

$$\text{Composite score} = \frac{Z_{\text{E2F}} + Z_{\text{G2M}} + Z_{\text{Mitotic spindle}}}{3}$$

A higher composite score represented greater activity of the coordinated proliferative transcriptional program.

2.5. Statistical Analysis

All statistical analyses were performed using R software (version 4.4.2), with R packages limma (3.60.6), fgsea (1.30.0), and GSVA (2.0.2). Hallmark gene sets were obtained from MSigDB version 7.5.1. The correlations among the three pathway scores were assessed using Spearman rank correlation to evaluate their concordance within the proliferative program. Because the underlying Hallmark sets overlap, correlation among their scores was interpreted as evidence of a shared transcriptional axis rather than independence among the three components. Shared-gene counts were taken from the archived Hallmark gene set membership; the comparison of the three single-pathway scores with the equal-weight composite was used to examine the sensitivity of the grade association to this overlap.

Differences in composite proliferative program scores between pathological grade groups were evaluated using the Wilcoxon rank-sum test. Grade-associated differences within each histological subtype were evaluated separately for gastric-type IPMN (gIPMN) and intestinal-type IPMN (iIPMN). Separate within-subtype hypothesis tests were treated as descriptive subgroup comparisons and were not interpreted as formal evidence of a difference in grade effects between histological subtypes. Two-sided exact Wilcoxon rank-sum tests were applied to 12 low-grade and 12 high-grade IPMN specimens overall and to six lesions per grade within each histological subtype. Prespecified score-construction sensitivity analyses assigned one-half weight to a single component and one-quarter weight to each remaining component. Comparisons with the three single-pathway scores used apparent within-sample areas under the receiver operating characteristic curve; these estimates were descriptive and were not treated as external predictive validation. For GSE26647, grade regression at the focus level used patient-clustered standard errors for the 14 contributing patients, with an additional analysis restricted to noninvasive foci.

To determine whether pathological grade and histological subtype were independently associated with proliferative program activity, multivariable linear regression analysis was performed among gIPMN and iIPMN samples. The composite proliferative program score was used as the dependent variable, with pathological grade and histological subtype included as independent variables: A separate linear model added the grade-by-subtype interaction term. An additional sensitivity model adjusted the grade and subtype coefficients for an epithelial expression proxy computed as the mean of individually z-transformed EPCAM, KRT7, KRT8, KRT18, KRT19, and CDH1 expression values across the 24 IPMN samples. The marker panel was interpreted as an expression-derived surrogate rather than a pathological purity estimate.

$$\beta_0 + \beta_1(\text{Pathological grade}) + \beta_2(\text{Histological subtype}) + \varepsilon$$

High-grade lesions and gIPMN were used as the reference categories in the regression model. Regression coefficients (β), 95% confidence intervals (CIs), and p values were reported. All statistical tests were two-sided, and $p < 0.05$ was considered statistically significant. For the primary additive model, the original high-grade and gastric-type

reference parameterization was preserved. The alternative models used high-grade indicator coding to facilitate interpretation of the grade contrast, with regression results based on the original archived composite scores.

3. Results

The overall analytical workflow and the characteristics of the three independent transcriptomic cohorts are summarized in Figure 1. GSE63104 was used as the discovery cohort to identify transcriptional programs associated with high-risk IPMN lesions, while GSE26647 served as an independent replication cohort. The GSE210351 cohort was subsequently analyzed for sample-level pathway activity and associations with pathological grade and histological subtype. Sample sizes and pathological group definitions for each cohort are reported in Table 1; the GSE210351 grade comparisons included 12 low-grade and 12 high-grade IPMN lesions.

3.1. Identification of a Conserved Proliferative Transcriptional Program Associated with Pathological Grade in IPMN

To identify transcriptional programs associated with the pathological progression of IPMN, gene set enrichment analysis (GSEA) was first performed in the discovery cohort GSE63104. Among the significantly enriched Hallmark pathways, three cell-cycle- and mitosis-related pathways showed consistent positive enrichment in high-risk IPMN, including HALLMARK_E2F_TARGETS, HALLMARK_G2M_CHECKPOINT, and HALLMARK_MITOTIC_SPINDLE (Figure 2A–C). The archived full Hallmark analysis yielded 14 FDR-significant sets in GSE63104, of which nine had positive enrichment and five negative enrichment. The full ranked results are provided in Supplementary Table S2. The selected pathways therefore represent a biologically interpreted subset of a wider FDR-significant transcriptional response rather than the only enriched Hallmark programs.

HALLMARK_E2F_TARGETS showed the strongest enrichment, with a normalized enrichment score (NES) of 2.90 and a false discovery rate (FDR) of 4.96×10^{-25}. HALLMARK_G2M_CHECKPOINT was similarly strongly enriched (NES = 2.78, FDR = 3.62×10^{-22}), while HALLMARK_MITOTIC_SPINDLE also showed significant positive enrichment (NES = 1.93, FDR = 1.59×10^{-6}). These very small gene set FDR values arise from enrichment testing on gene-level rankings and should not be interpreted as patient-level replication probabilities or as estimates calibrated by cohort size.

The enrichment curves demonstrated coordinated accumulation of genes belonging to these pathways toward the leading edge of the ranked gene lists, indicating increased representation of E2F-regulated cell-cycle activity, G2/M checkpoint processes, and mitotic spindle-associated programs in high-risk IPMN. Because these three pathways collectively represented a coherent proliferative pattern, they were defined as the core proliferative transcriptional program for subsequent validation analyses. Shared leading-edge genes and core pathway membership overlaps are summarized in Supplementary Table S7. Leading-edge lists saved with the original fgsea objects identified AURKA, BIRC5, CCNB2, CENPE, and PLK1 in all three core pathways in both cohorts. These recurrent leading-edge genes provide specific candidates for subsequent compartment-resolved validation. Their presence in multiple sets also illustrates why the three Hallmark scores should not be interpreted as independent biological predictors.

3.2. Independent Replication of Proliferative Transcriptional Enrichment

To evaluate the reproducibility of the identified proliferative program, an independent IPMN transcriptomic cohort, GSE26647, was analyzed. Consistent with the discovery cohort, all three core pathways showed concordant positive enrichment patterns in high-risk

lesions, with consistent enrichment directions across the two cohorts (Table 2). HALLMARK_E2F_TARGETS showed an NES of 3.31 (FDR = 1.54×10^{-26}), followed by HALLMARK_G2M_CHECKPOINT (NES = 2.94, FDR = 4.39×10^{-19}) and HALLMARK_MITOTIC_SPINDLE (NES = 2.69, FDR = 1.13×10^{-14}). The common finding across datasets was positive enrichment of these pathways; differences in NES magnitude were not treated as effect-size comparisons between cohorts using different platforms and sample structures. GSE26647 included laser-capture microdissected pathological foci, providing an anatomically enriched comparison alongside the bulk tissue discovery cohort. All 50 Hallmark pathways from the original GSE26647 enrichment analysis are tabulated in Supplementary Table S3; 40 met the FDR threshold of 0.05, comprising 39 positively enriched pathways and one negatively enriched pathway.

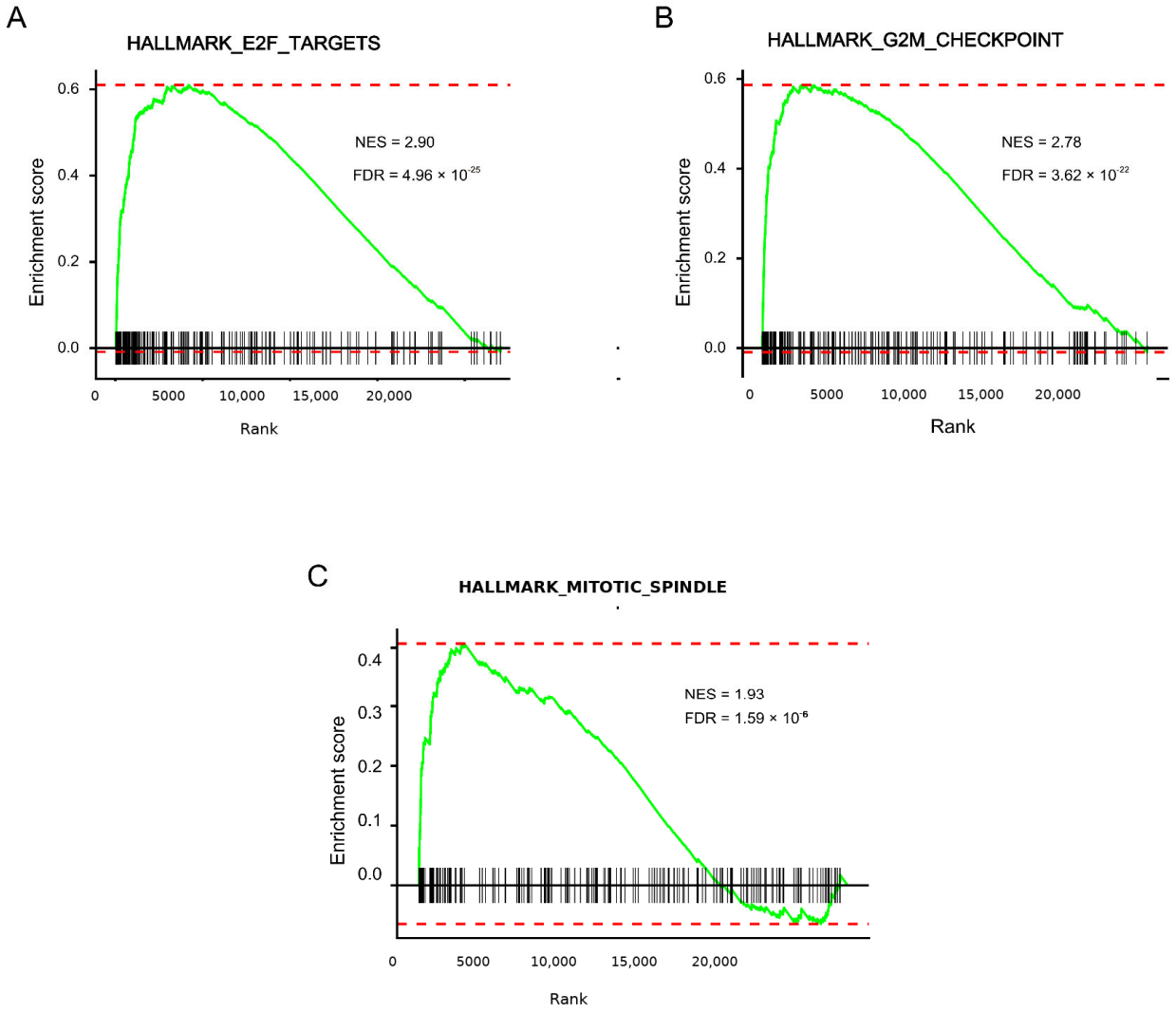

Figure 2. Identification of a proliferative transcriptional program in IPMN using Hallmark gene set enrichment analysis (**A**–**C**) Gene set enrichment analysis (GSEA) was performed in the discovery cohort (GSE63104) to identify cell cycle- and mitosis-associated transcriptional programs enriched in high-risk versus low-risk IPMN samples. Three significantly enriched Hallmark gene sets are shown: (**A**) HALLMARK_E2F_TARGETS, (**B**) HALLMARK_G2M_CHECKPOINT, and (**C**) HALLMARK_MITOTIC_SPINDLE. Each panel displays the enrichment curve illustrating the distribution of pathway-associated genes along the ranked gene list. Normalized enrichment score (NES) and false discovery rate (FDR) values are annotated for each gene set. The solid green curves show the running enrichment scores, black ticks mark gene-set members along the ranked gene lists, and red dashed lines are plot reference guides.

Table 2. Enrichment of three cell-cycle Hallmark pathways in the discovery and independent cohorts. Positive normalized enrichment scores indicate enrichment in the higher-grade or higher-risk category. NES values are reported within each cohort and are not interpreted as directly comparable effect sizes across different platforms and sample structures.

Hallmark Pathway	GSE63104 NES	GSE63104 FDR	GSE26647 NES	GSE26647 FDR
E2F targets	2.902	4.96×10^{-25}	3.309	1.54×10^{-26}
G2M checkpoint	2.782	3.62×10^{-22}	2.939	4.39×10^{-19}
Mitotic spindle	1.933	1.59×10^{-6}	2.691	1.13×10^{-14}

These findings support the recurrence of positive cell-cycle pathway enrichment in two independent pathological series. The independent specimen-level analysis reported below provides a separate test of the grade association, while absolute cross-platform score transfer and clinical prediction remain outside the scope of the enrichment comparisons.

3.3. Association of the Proliferative Program with Pathological Grade and Histological Subtype

To further evaluate the association of the proliferative program with pathological characteristics at the individual-sample level, an independent cohort, GSE210351, was analyzed. Sample-level ssGSEA scores were calculated for HALLMARK_E2F_TARGETS, HALLMARK_G2M_CHECKPOINT, and HALLMARK_MITOTIC_SPINDLE, and the three pathway scores were positively correlated within the 24 IPMN specimens, with correlation coefficients provided in Supplementary Table S7. These standardized pathway scores were therefore integrated into a composite score representing the shared proliferative transcriptional program. The overlapping membership of the three Hallmark sets was considered in interpreting the composite as a coordinated transcriptional summary. Across the 24 IPMN specimens, the original standardized E2F and G2M scores had a Spearman correlation of 0.932, compared with 0.540 for E2F and spindle and 0.661 for G2M and spindle. The archived Hallmark membership lists contained 73 genes common to E2F and G2M, 19 common to E2F and spindle, and 39 common to G2M and spindle, confirming substantive membership overlap; see Supplementary Table S7.

Across all IPMN samples, high-grade lesions exhibited significantly higher composite program scores than low-grade lesions (Figure 3A; $p = 0.0029$). This finding indicates that greater activity of the proliferative transcriptional program was associated with higher pathological grades. The comparison involved 12 low-grade and 12 high-grade lesions. Verification against the archived individual scores reproduced the two-sided exact Wilcoxon test with U = 22 for the low-grade group and $p = 0.002914$. The median composite score was −0.834 in low-grade lesions and 0.193 in high-grade lesions.

We next examined the association between the composite score and pathological grade within histological subtypes. In gIPMN, high-grade lesions showed significantly higher composite scores than low-grade lesions (Figure 3B; $p = 0.0022$). In iIPMN, the composite score showed a similar upward trend in high-grade lesions, although the difference did not reach statistical significance (Figure 3C; $p = 0.3095$). With six lesions in each subtype-grade cell, the subgroup comparisons were interpreted descriptively and the formal interaction test was prioritized when assessing heterogeneity by histological subtype. Each histological subtype contained six low-grade and six high-grade lesions. The difference in subgroup significance was interpreted as a difference in statistical evidence, not as proof of a grade-by-subtype interaction. In the original archived scores, the gastric-type comparison yielded an exact rank-sum p value of 0.002165 with low-grade U = 0. The intestinal-type comparison yielded U = 11 and $p = 0.309524$. Both comparisons included six low-grade and six high-grade lesions, and the original plotted scores were retained.

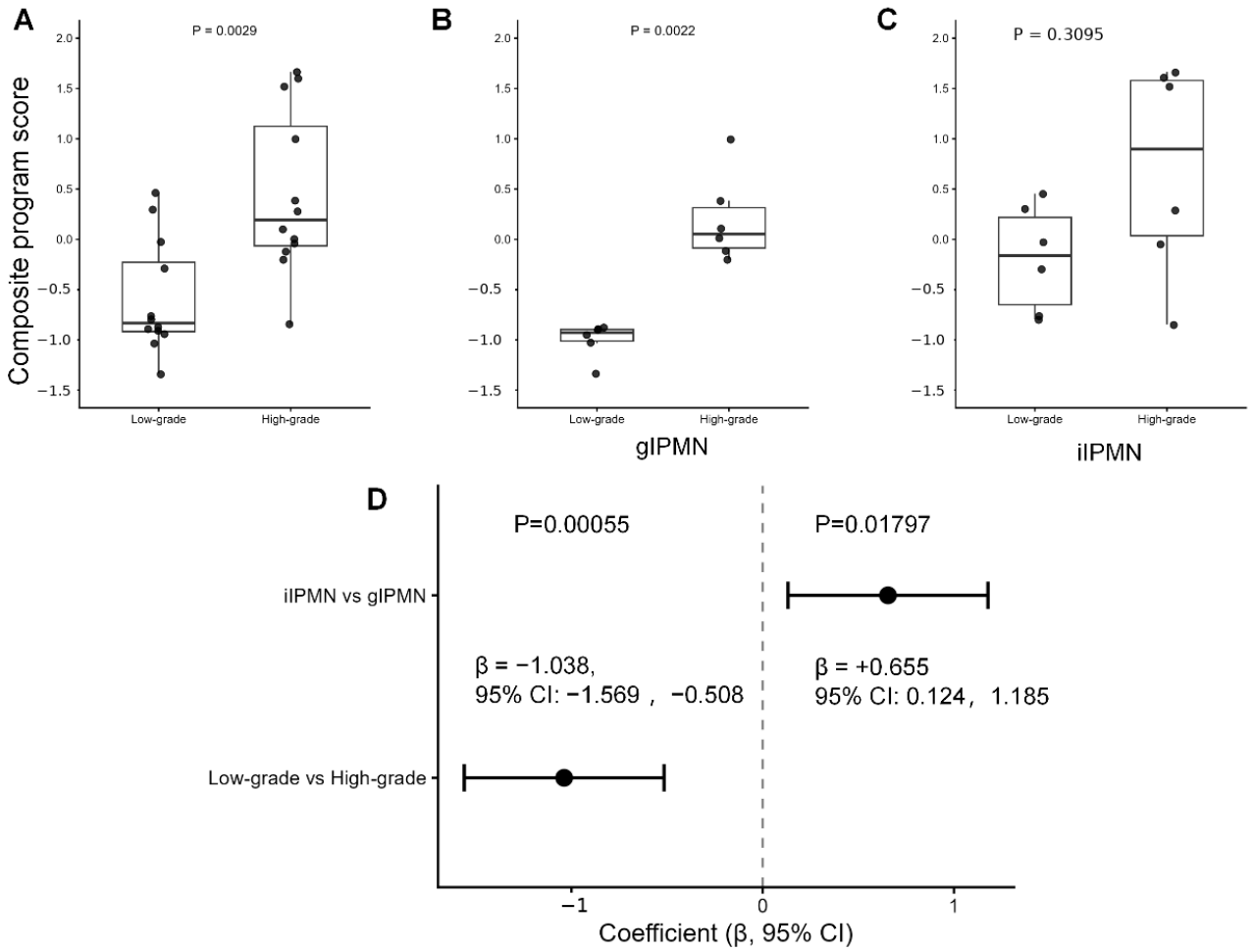

Figure 3. Association between the proliferative transcriptional program and pathological characteristics of IPMN. (**A**) Box plot comparing composite proliferative program scores between low-grade and high-grade IPMN lesions in the overall cohort. Composite scores were significantly higher in high-grade lesions compared with low-grade lesions. (**B**,**C**) Subgroup analyses stratified by histological subtype. (**B**) In gastric-type IPMN (gIPMN), composite proliferative program scores were significantly higher in high-grade lesions compared with low-grade lesions. (**C**) In intestinal-type IPMN (iIPMN), composite scores showed a similar increasing trend in high-grade lesions, although the difference did not reach statistical significance. (**D**) Multivariable linear regression analysis assessing the associations of pathological grade and histological subtype with composite proliferative program scores. The plot displays regression coefficients (β) and corresponding 95% confidence intervals (CIs). High-grade lesions and gIPMN were used as reference categories for pathological grade and histological subtype, respectively. The comparisons involved 12 low-grade and 12 high-grade lesions in panel (**A**); six low-grade and six high-grade gastric-type lesions in panel (**B**); and six low-grade and six high-grade intestinal-type lesions in panel (**C**). The respective two-sided *p* values were 0.0029, 0.0022, and 0.3095. Panel (**D**) includes 24 IPMN lesions, with 12 lesions per histological subtype; the displayed regression coefficients refer to the additive model.

To determine whether the association between the proliferative program and pathological grade remained after accounting for histological subtype, multivariable linear regression was performed among gIPMN and iIPMN samples (Figure 3D). Using high-grade lesions and gIPMN as the reference categories, low-grade IPMN was associated with a significantly lower composite program score (β = −1.038, 95% CI: −1.569 to −0.508, $p = 0.00055$). In addition, iIPMN was associated with a higher composite score than gIPMN after adjustment for pathological grade (β = 0.655, 95% CI: 0.124 to 1.185, $p = 0.01797$).

Together, these findings indicate that the association between the proliferative transcriptional program and pathological grade remained significant after adjustment for histological subtype, and the fitted additive model also showed an average score difference by histological subtype. In the formal interaction model, the grade-by-intestinal-subtype coefficient was −0.310, 95% CI −1.391 to 0.771, $p = 0.5568$. Thus, the difference between the gastric-type and intestinal-type subgroup p values did not constitute evidence of different grade effects by subtype.

3.4. Additional Sensitivity Analyses and Cross-Cohort Reproducibility

GSE26647 provided an independent pathology-stratified sensitivity analysis at the individual-focus level. In all 28 microdissected foci from 14 patients, the higher-risk versus lower-risk composite contrast was 0.996, 95% CI 0.391 to 1.600, $p = 0.00351$ using patient-clustered t inference. After removing seven invasive cancer foci, six high-grade noninvasive foci were compared with 15 low-grade or moderate-grade foci from the same 14 patients. The grade contrast remained positive at 1.298, 95% CI 0.601 to 1.996, $p = 0.00145$. In the noninvasive subset, E2F, G2M, and spindle contrasts were 1.449, 1.479, and 0.967 with cluster-adjusted p values of 0.000758, 0.00190, and 0.0186, respectively. Three patients had both a high-grade noninvasive and a lower-grade focus; all three showed a positive within-patient composite contrast. These observations extend the enrichment-direction replication while accounting for the nonindependence of tissue foci from the same patient. Details are reported in Supplementary Table S4.

Comparison of the original 24-sample composite with its individual pathway components support the equal-weight index as a descriptive summary rather than an optimized classifier. The apparent grade-discrimination area under the curve was 0.847 for the equal-weight score, 0.785 for E2F alone, 0.847 for G2M alone, and 0.833 for spindle alone. Three alternatives giving one-half weight to E2F, G2M, or spindle yielded apparent areas of 0.840, 0.854, and 0.868, respectively. Across these prespecified weighting choices, the exact rank-sum p values ranged from 0.00143 to 0.00364, supporting a consistent direction of grade association without establishing a uniquely optimal set of coefficients. Full estimates are shown in Supplementary Table S5. An overview of the noninvasive focus-level comparisons and the alternative-weight AUC estimates is provided in Supplementary Figure S1.

The GSE210351 epithelial marker expression proxy was introduced into the additive pathological grade and subtype model as a sensitivity covariate. The high-grade coefficient remained positive at 1.068, 95% CI 0.530 to 1.605, $p = 0.000502$, compared with 1.038 in the original additive model. The epithelial marker proxy coefficient was 0.201, $p = 0.355$. These estimates indicate that the grade association was retained after this expression-based adjustment, without equating the marker proxy with a direct morphometric assessment of tumor epithelial content. The interaction and epithelial-adjusted regression estimates are reported in Supplementary Table S6.

4. Discussion

In this study, we performed a multi-cohort transcriptomic analysis to identify and replicate enrichment of transcriptional programs associated with pathological progression of IPMNs. By integrating differential expression analysis, Hallmark gene set enrichment analysis, independent cohort enrichment comparisons, and sample-level pathway quantification, we identified a conserved proliferative transcriptional program characterized by coordinated activation of E2F targets, G2M checkpoint, and mitotic spindle pathways. This program demonstrated consistent enrichment patterns across independent transcriptomic cohorts and showed significant associations with pathological grade, particularly in the overall IPMN cohort and within the gastric-type IPMN subgroup. Furthermore, multivari-

able analysis indicated that pathological grade remained independently associated with proliferative program activity after adjustment for histological subtype. Together, these findings suggest that pathway-level assessment of coordinated proliferative activity may capture molecular features associated with IPMN progression beyond individual gene-level expression changes.

The identification of a proliferative transcriptional program in this study is consistent with previous molecular studies indicating that cell-cycle deregulation represents an important feature accompanying neoplastic progression in IPMNs. Integrated molecular characterization of IPMNs has demonstrated that high-grade lesions exhibit transcriptional activation of oncogenic programs, including E2F targets and cell-cycle-associated pathways, supporting the involvement of coordinated proliferative processes during progression toward malignancy [4]. Beyond IPMN-specific studies, E2F transcription factors are recognized as central regulators of cell-cycle progression and cancer-associated proliferation. E2F proteins coordinate the expression of genes involved in DNA replication, DNA repair, checkpoint control, chromosome segregation, and mitotic progression. Previous mechanistic studies have demonstrated that E2F directly regulates a broad network of cell-cycle genes, linking E2F activity with DNA replication and G2/M checkpoint regulation [8]. More recent studies have further emphasized the role of dysregulated E2F activity in sustaining proliferative states and promoting tumor progression through persistent activation of cell-cycle transcriptional programs [9,10]. Therefore, the coordinated enrichment of E2F targets, G2M checkpoint, and mitotic spindle pathways observed across independent IPMN cohorts may represent a transcriptional manifestation of increased proliferative activity during pathological progression.

The coordinated increase in replication-associated E2F transcription, checkpoint activity, and spindle organization offers a phase-resolved description of the high-grade proliferative state. Individual leading-edge cell-cycle genes may be useful candidates for targeted tissue-level assessment, but their contribution to IPMN biology should be established by cell-type-resolved expression analysis and functional experiments. The principal contribution of the present analysis is the reproducibility of a coordinated transcriptional pattern in independent pathological series rather than the discovery of a previously unrecognized proliferative pathway. Original leading-edge evidence from two independent GEO comparisons further concentrated the replicated signal in AURKA, BIRC5, CCNB2, CENPE, and PLK1 across all three pathways. AURKA and PLK1 regulate mitotic transitions, BIRC5 participates in chromosome segregation and survival signaling, and CENPE is involved in kinetochore function. Within the present study, these molecules are prioritized as reproducibly enriched components for immunohistochemical or spatial testing rather than established drug targets in IPMN.

An important aspect of the present study is the identification of a pathway-level proliferative program rather than reliance on individual differentially expressed genes. Although gene-level analyses can reveal specific molecular alterations associated with disease progression, biological processes such as cell-cycle regulation are typically controlled by coordinated changes involving multiple functionally related genes. Therefore, pathway-based approaches may provide a more robust representation of biological states by integrating expression patterns across gene sets. The Hallmark gene sets used in this study were specifically developed to represent well-defined biological processes with reduced redundancy compared with broader pathway collections, enabling more interpretable assessment of transcriptional programs [11]. In addition, sample-level approaches, such as single-sample gene set enrichment analysis, allow quantitative estimation of pathway activity in individual samples, facilitating comparisons across heterogeneous clinical and molecular subgroups [12]. By combining pathway discovery, independent enrichment

assessment, and sample-level scoring, our study demonstrates that coordinated proliferative activity can be reproducibly evaluated across independent IPMN cohorts, providing a complementary framework to traditional gene-centric analyses.

Unlike Ki-67 immunohistochemistry, which estimates the fraction of immunoreactive cycling cells within a selected histological compartment, the transcriptomic score integrates the relative abundance of multiple cell-cycle transcripts in a tissue specimen. This distinction offers a potential route to molecular characterization across heterogeneous specimens, although the present data do not establish incremental discrimination beyond Ki-67 or other histological measures. The equal-weight score is therefore regarded as a compact representation of transcriptional activity, not an independently validated clinical classifier. The archived-score comparison showed a composite apparent AUC of 0.847, equivalent to G2M alone and below the spindle-emphasized weighting of 0.868. Thus, the added value of the composite lies in consistent and interpretable summarization of coordinated gene set activity, not demonstrated superiority in discrimination. A direct comparison with Ki-67 requires measurements on the same specimens and prespecified performance evaluation.

IPMNs represent a heterogeneous group of precursor lesions with distinct molecular and biological characteristics, and increasing evidence suggests that pathological progression does not follow a uniform evolutionary trajectory. Recent genomic and transcriptomic studies have demonstrated substantial heterogeneity among IPMN subtypes, with gastric-type and intestinal-type lesions exhibiting distinct molecular profiles and patterns of progression toward malignancy [13,14]. Spatial transcriptomic analyses have further revealed subtype-specific transcriptional programs associated with different stages of IPMN progression, including alterations involving MYC activation, inflammatory signaling, and cell-cycle-related pathways [15]. In the present study, the within-subtype grade comparison reached statistical significance in gastric-type IPMN and showed a concordant direction in intestinal-type IPMN, where the comparison was less precise. The observed pattern is compatible with proliferation-associated transcriptional changes arising in distinct gastric-type and intestinal-type molecular backgrounds; it does not by itself establish a subtype-specific difference in the grade effect. Given the limited number of samples in subtype-stratified analyses, further studies integrating larger cohorts and multi-dimensional molecular profiling are required to clarify the relationship between proliferative programs and IPMN subtype evolution.

The adjusted positive coefficient for intestinal-type IPMN indicates a higher average composite score at a given pathological grade in the fitted additive model. This subtype main effect is distinct from a grade-by-subtype interaction. Reported differences in within-subtype p values therefore warrant a cautious interpretation, particularly because each subtype-grade cell contained six lesions. The grade-by-subtype interaction coefficient of −0.310 was compatible with both a modest negative and a positive subtype modification of the grade effect, and its p value of 0.5568 did not support a statistically established interaction. The positive grade trend within intestinal-type IPMN therefore remains biologically compatible with the overall association despite the imprecise six-versus-six subgroup test.

From a clinical perspective, improving the accuracy of IPMN risk assessment remains an important challenge. Current management strategies primarily rely on imaging characteristics, clinical features, and pathological findings according to international consensus guidelines [3], which provide valuable guidance but may not fully capture the underlying biological heterogeneity of individual lesions. Recent transcriptomic and spatial profiling studies have demonstrated that IPMNs with similar pathological classifications may contain distinct molecular states associated with different malignant potentials [15,16]. These findings highlight the potential value of incorporating molecular information into conventional risk assessment frameworks. In this context, the present study provides evidence that cell-

cycle pathway enrichment recurs across independent pathological cohorts and that higher composite scores are associated with higher pathological grade in the studied specimens. A clinical application would require a fixed preprocessing and scoring reference, independent patient-level evaluation, and direct comparison with established pathological measures.

A distinction is required between cross-sectional pathological classification and prospective malignant transformation. The available cohorts compared lesions already assigned different histological grades, and enrichment-direction replication did not measure sensitivity, specificity, calibration, or future clinical events. The identified signal is best regarded as a pathology-associated transcriptional phenotype whose complementary clinical utility can be assessed against routine proliferation markers in well-annotated prospective collections. The original GSE26647 enrichment analysis also encompassed 40 FDR-significant Hallmark gene sets, so the proliferative program was situated within broader metabolic and microenvironmental differences rather than presented as a unique initiating mechanism. The five repeatedly detected leading-edge genes highlight testable candidate processes but do not demonstrate functional causation, prospective risk classification, or therapeutic efficacy.

5. Limitations

Several limitations should be considered when interpreting the findings of this study. First, although we integrated multiple independent public transcriptomic cohorts, the retrospective nature of these datasets and differences in sample composition, platform characteristics, and pathological annotation may introduce potential sources of variability. Second, the current analysis was based on bulk transcriptomic profiles, which reflect the averaged expression patterns of heterogeneous tissue components and cannot fully distinguish the contributions of epithelial, stromal, and immune cell populations. Future studies incorporating single-cell or spatial transcriptomic approaches may help determine the cellular origin and biological context of the identified proliferative program. Third, subtype-stratified analyses, particularly within intestinal-type IPMN, were limited by sample size and require validation in larger independent cohorts. Finally, although the identified transcriptional program showed reproducible associations with pathological progression, functional experiments will be necessary to determine whether these proliferative pathways actively contribute to IPMN evolution or represent molecular indicators of disease progression. The relative epithelial content of bulk specimens is a specific potential source of confounding because a higher fraction of proliferating lesional epithelium can increase a tissue-level cell-cycle score independently of per-cell pathway activity. Concordant enrichment in the laser-capture microdissected GSE26647 series provides complementary evidence from histologically selected foci, but it is not a quantitative adjustment for epithelial or tumor cellularity. Accordingly, the program is interpreted here as a tissue-level transcriptional phenotype. The strong biological overlap among the three Hallmark components likewise means that the equal-weight index summarizes shared cell-cycle regulation rather than three independent signals. Multiple histological foci from the same patient in GSE26647 also limit the independence of that series and emphasize the descriptive nature of the cross-cohort enrichment comparison. The additional patient-clustered noninvasive sensitivity analysis reduced dependence on the invasive-lesion grouping, although only three patients contributed a high-grade and lower-grade noninvasive pair. An epithelial marker proxy was associated with imprecisely measured tissue cellularity and could not replace pathologist-estimated tumor fraction or spatially resolved cell-type-specific expression. Finally, the original GSVA scores were standardized across all 41 specimens before analyzing the 24 IPMN lesions; the numeric scale is specific to that reference distribution, while the reported rank-based group comparisons retain the archived analysis definition.

Consequently, the present score is unsuitable for uncalibrated individual patient application, and the external focus-level sensitivity analysis should be distinguished from transfer of the original numerical score. The available supporting documents do not provide a recoverable, threshold-defined inventory of differentially expressed genes for the two microarray comparisons; the reported inference therefore rests on the archived full gene set enrichment results.

6. Conclusions

In conclusion, this multi-cohort transcriptomic study identified a recurring grade-associated proliferative transcriptional pattern characterized by coordinated activation of E2F targets, G2M checkpoint, and mitotic spindle pathways across independent IPMN datasets. The activity of this program was associated with pathological grade, with the overall association retained in an epithelial-marker-adjusted model and in a noninvasive focus-level sensitivity analysis. These findings highlight the potential value of pathway-level transcriptomic analysis for characterizing molecular features associated with IPMN progression and support further cell-type-resolved and pathology-controlled evaluation of transcriptional proliferation in IPMN. Sensitivity analyses excluding invasive foci and adjusting for an epithelial marker expression score supported the grade-related transcriptional association. The interaction test did not establish a different grade effect between gastric-type and intestinal-type lesions, and alternative weighting did not demonstrate unique superiority of the equal-weight composite. These findings establish a reproducible direction of cell-cycle pathway enrichment across the studied pathological contrasts and identify mitotic leading-edge candidates for tissue compartment assessment, without establishing clinical predictive performance.

Supplementary Materials: The following supporting information can be downloaded at: https://www.mdpi.com/article/10.3390/genes17121532/s1. Supplementary Table S1. Cohorts and pathological group definitions; Supplementary Table S2. All 50 Hallmark pathways in GSE63104; Supplementary Table S3. All 50 Hallmark pathways in GSE26647; Supplementary Table S4. Patient-clustered GSE26647 sensitivity contrasts; Supplementary Table S5. Equal, reweighted, and individual pathway comparisons in GSE210351; Supplementary Table S6. Original-score linear models in 24 IPMN lesions; Supplementary Table S7. Original cross-cohort leading-edge gene recurrence; Figure S1. Original-score sensitivity summary.

Author Contributions: Conceptualization, H.R. and Z.J.; methodology, formal analysis, and writing—original draft preparation, H.R.; investigation and writing—review and editing, Q.C.; supervision and writing—review and editing, Z.J. All authors have read and agreed to the published version of the manuscript.

Funding: This research received no external funding.

Institutional Review Board Statement: Not applicable, as this study analyzed publicly available transcriptomic datasets and did not involve the collection of new human samples or identifiable patient data.

Informed Consent Statement: Not applicable.

Data Availability Statement: The datasets analyzed in this study are publicly available from the Gene Expression Omnibus (GEO) database under accession numbers GSE63104, GSE26647, and GSE210351. The original GEO series records also provide platform information and sample-level accession identifiers. The accompanying Supplementary Methods and Results document provides cohort definitions, full Hallmark enrichment rankings, the original score comparison summaries, and sensitivity model estimates. The archived original analysis workspace and executable R scripts should be requested from the corresponding author if independent computational reproduction is required.

Conflicts of Interest: The authors declare no conflicts of interest.

References

1. Vilela, A.; Quingalahua, E.; Vargas, A.; Hawa, F.; Shannon, C.; Carpenter, E.S.; Shi, J.; Krishna, S.G.; Lee, U.-J.; Chalhoub, J.M.; et al. Global Prevalence of Pancreatic Cystic Lesions in the General Population on Magnetic Resonance Imaging: A Systematic Review and Meta-analysis. *Clin. Gastroenterol. Hepatol.* **2024**, *22*, 1798–1809.e6. [CrossRef] [PubMed] [PubMed Central]
2. Pollini, T.; Wong, P.; Maker, A.V. The Landmark Series: Intraductal Papillary Mucinous Neoplasms of the Pancreas—From Prevalence to Early Cancer Detection. *Ann. Surg. Oncol.* **2023**, *30*, 1453–1462. [CrossRef] [PubMed] [PubMed Central]
3. Tanaka, M.; Fernández-del Castillo, C.; Kamisawa, T.; Jang, J.Y.; Levy, P.; Ohtsuka, T.; Salvia, R.; Shimizu, Y.; Tada, M.; Wolfgang, C.L. Revisions of international consensus Fukuoka guidelines for the management of IPMN of the pancreas. *Pancreatology* **2017**, *17*, 738–753. [CrossRef] [PubMed]
4. Semaan, A.; Bernard, V.; Wong, J.W.; Makino, Y.; Swartzlander, D.B.; Rajapakshe, K.I.; Lee, J.J.; Officer, A.; Schmidt, C.M.; Wu, H.H.; et al. Integrated Molecular Characterization of Intraductal Papillary Mucinous Neoplasms: An NCI Cancer Moonshot Precancer Atlas Pilot Project. *Cancer Res. Commun.* **2023**, *3*, 2062–2073. [CrossRef] [PubMed] [PubMed Central]
5. Bernard, V.; Semaan, A.; Huang, J.; Lucas, F.A.S.; Mulu, F.C.; Stephens, B.M.; Guerrero, P.A.; Huang, Y.; Zhao, J.; Kamyabi, N.; et al. Single-Cell Transcriptomics of Pancreatic Cancer Precursors Demonstrates Epithelial and Microenvironmental Heterogeneity as an Early Event in Neoplastic Progression. *Clin. Cancer Res.* **2019**, *25*, 2194–2205. [CrossRef] [PubMed] [PubMed Central]
6. Fischer, C.G.; Beleva Guthrie, V.; Braxton, A.M.; Zheng, L.; Wang, P.; Song, Q.; Griffin, J.F.; Chianchiano, P.E.; Hosoda, W.; Niknafs, N.; et al. Intraductal Papillary Mucinous Neoplasms Arise From Multiple Independent Clones, Each With Distinct Mutations. *Gastroenterology* **2019**, *157*, 1123–1137.e22. [CrossRef] [PubMed] [PubMed Central]
7. Jury, R.P.; Thibodeau, B.J.; Fortier, L.E.; Geddes, T.J.; Ahmed, S.; Pruetz, B.L.; Farinola, M.A.; Wilson, G.D. Gene Expression Changes Associated With the Progression of Intraductal Papillary Mucinous Neoplasms. *Pancreas* **2012**, *41*, 611–618. [CrossRef] [PubMed]
8. Ren, B.; Cam, H.; Takahashi, Y.; Volkert, T.; Terragni, J.; Young, R.A.; Dynlacht, B.D. E2F integrates cell cycle progression with DNA repair, replication, and G_2/M checkpoints. *Genes Dev.* **2002**, *16*, 245–256. [CrossRef] [PubMed] [PubMed Central]
9. Kent, L.N.; Leone, G. The broken cycle: E2F dysfunction in cancer. *Nat. Rev. Cancer* **2019**, *19*, 326–338. [CrossRef] [PubMed]
10. Pennycook, B.R.; Vesela, E.; Peripolli, S.; Singh, T.; Barr, A.R.; Bertoli, C.; de Bruin, R.A.M. E2F-dependent transcription determines replication capacity and S phase length. *Nat. Commun.* **2020**, *11*, 3503. [CrossRef] [PubMed] [PubMed Central]
11. Liberzon, A.; Birger, C.; Thorvaldsdóttir, H.; Ghandi, M.; Mesirov, J.P.; Tamayo, P. The Molecular Signatures Database (MSigDB) Hallmark Gene Set Collection. *Cell Syst.* **2015**, *1*, 417–425. [CrossRef] [PubMed] [PubMed Central]
12. Hänzelmann, S.; Castelo, R.; Guinney, J. GSVA: Gene set variation analysis for microarray and RNA-seq data. *BMC Bioinform.* **2013**, *14*, 7. [CrossRef] [PubMed] [PubMed Central]
13. Liffers, S.-T.; Godfrey, L.; Frohn, L.; Haeberle, L.; Yavas, A.; Vesce, R.; Goering, W.; Opitz, F.V.; Stoecklein, N.; Knoefel, W.T.; et al. Molecular heterogeneity and commonalities in pancreatic cancer precursors with gastric and intestinal phenotype. *Gut* **2022**, *72*, 522–534. [CrossRef] [PubMed] [PubMed Central]
14. Basturk, O.; Hong, S.-M.; Wood, L.D.; Adsay, N.V.; Albores-Saavedra, J.; Biankin, A.V.; Brosens, L.A.; Fukushima, N.; Goggins, M.; Hruban, R.H.; et al. A Revised Classification System and Recommendations From the Baltimore Consensus Meeting for Neoplastic Precursor Lesions in the Pancreas. *Am. J. Surg. Pathol.* **2015**, *39*, 1730–1741. [CrossRef] [PubMed] [PubMed Central]
15. Agostini, A.; Piro, G.; Inzani, F.; Quero, G.; Esposito, A.; Caggiano, A.; Priori, L.; Larghi, A.; Alfieri, S.; Casolino, R.; et al. Identification of spatially-resolved markers of malignant transformation in Intraductal Papillary Mucinous Neoplasms. *Nat. Commun.* **2024**, *15*, 2764. [CrossRef] [PubMed] [PubMed Central]
16. Iyer, M.K.; Fletcher, A.A.; Okoye, J.O.; Shi, C.; Chen, F.; Kanu, E.N.; Eckhoff, A.M.; Bao, M.; di Magliano, M.P.; Frankel, T.L.; et al. Spatial Transcriptomics of Intraductal Papillary Mucinous Neoplasms Reveals Divergent Indolent and Malignant States. *Clin. Cancer Res.* **2025**, *31*, 1796–1808. [CrossRef] [PubMed] [PubMed Central]

Disclaimer/Publisher's Note: The statements, opinions and data contained in all publications are solely those of the individual author(s) and contributor(s) and not of MDPI and/or the editor(s). MDPI and/or the editor(s) disclaim responsibility for any injury to people or property resulting from any ideas, methods, instructions or products referred to in the content.